

Contents lists available at ScienceDirect

Organic Geochemistry

journal homepage: www.elsevier.com/locate/orggeochem



Novel methyl-branched alkenones with up to five double bonds in saline lakes



Sian Liao ^{a,b}, Karen J. Wang ^{b,c}, Yazhen Xue ^d, Jingfeng Huo ^d, Ewerton Santos ^c, Jianbo Wang ^d, Carsten J. Schubert ^e, Yongsong Huang ^{c,*}

- ^a Department of Chemistry, Brown University, 324 Brook Street, Providence, RI 02912, USA
- ^b Institute at Brown for Environment and Society, Brown University, Providence, RI 02912, USA
- ^cDepartment of Earth, Environmental and Planetary Sciences, Brown University, 324 Brook Street, Providence, RI 02912, USA
- ^d Beijing National Laboratory of Molecular Sciences (BNLMS) and Key Laboratory of Bioorganic Chemistry and Molecular Engineering of Ministry of Education, College of Chemistry, Peking University, Beijing 100871, China
- ^e Eawag, Swiss Federal Institute of Aquatic Science and Technology, Department of Surface Waters Research and Management, 6047 Kastanienbaum, Switzerland

ARTICLE INFO

Article history: Received 6 February 2021 Received in revised form 23 April 2021 Accepted 27 April 2021 Available online 8 May 2021

Keywords: α-methyl-branched alkenones Lake Van Isochrysidales Mass spectrometry Double bond position

ABSTRACT

Long-chain alkenones, a class of highly specific and widely used lipid biomarkers found in ocean and lake sediments, have been so far found as straight-chain alkyl ketones with 2 to 4 double bonds. Jaraula et al. (2010) reported assignments of a series of tri- to penta-unsaturated alkenones as straight-chain C38 methyl (C₃₈Me) and C₃₉ ethyl (C₃₉Et) alkenones in Lake Fryxell, Antarctica. The same series of compounds were later found in sediments from Lake Van (Randlett et al., 2014). The structure assignments by Jaraula et al (2010) were primarily based on strong ions at $[M-43]^+$ for C_{38} alkenones and $[M-57]^+$ for C_{39} alkenones, which were interpreted as a loss of CH₃CO and CH₃CH₂CO groups. However, such fragmentation is atypical for common straight-chain methyl and ethyl alkenones. In this study, we reanalyzed Lake Van sediment samples. We show these new C₃₈ and C₃₉ alkenones elute earlier than the common straightchain C_{38} Me and C_{39} Et alkenones on a mid-polarity GC column. After hydrogenation, mass spectra of these new alkenones show distinct peaks at m/z 72 or 86 caused by McLafferty rearrangement, indicating a methyl substitution at the α position of the carbonyl group in these C_{38} and C_{39} alkenones (i.e., α methyl-branched C₃₈Me and C₃₉Et). Our new assignments as methyl-branched alkenones are further confirmed by the synthesis of an analog α -methyl C_{25} methyl ketone and comparison of mass spectra. Double bond positions for branched $C_{38:5}$ Me (br $C_{38:5}$ Me) are found to be Δ^4 , Δ^7 , Δ^{14} , Δ^{21} and Δ^{28} based on the mass spectrum of corresponding dimethyl disulfide adducts. Analysis of Lake Van alkenone data reveals that U_{br38Me}^{K*} based on brC_{38} Me shows a trend similar to U_{37}^{K} for the past 270 ka, suggesting that the degree of unsaturation of branched alkenones is also sensitive to temperature.

© 2021 Elsevier Ltd. All rights reserved.

1. Introduction

Alkenones are polyunsaturated long-chain (C_{37} to C_{42}) methyl and ethyl ketones exclusively produced by Isochrysidales, an order of haptophyte algae (Zheng et al., 2019; Liao et al., 2020). They are diagenetically highly stable and have been found in marine sediments of Cretaceous age (Farrimond et al., 1986; Brassell et al., 2004). Importantly, the degree of unsaturation of alkenones shows a strong linear relationship with growth temperatures of the algae (Brassell et al., 1986; Müller et al., 1998). For nearly 40 years, $U_{37}^{\rm K}$ and $U_{37}^{\rm K}$ indices based on the degree of unsaturation of C_{37} methyl

E-mail address: yongsong_huang@brown.edu (Y. Huang).

 $(C_{37}Me)$ alkenones have been widely used for reconstructing paleosea surface (e.g., Brassell et al., 1986; Rosell-Melé and Comes, 1999; Tzanova and Herbert, 2015) and lake surface temperatures (e.g., Liu et al., 2006; D'Andrea et al., 2011; Randlett et al., 2014; Longo et al., 2020).

All alkenones identified so far contain a straight alkyl chain with a carbonyl group at position 2 or 3 (methyl and ethyl ketones, respectively) and 2 to 4 double bonds (Zheng et al., 2019). However, Jaraula et al. (2010) reported a new series of C₃₈ and C₃₉ alkenones that contain 3 to 5 double bonds in surface sediments from Lake Fryxell, Antarctica. The same series of compounds were later found in sediments from Lake Van, Turkey (Randlett et al., 2014). Mass spectra of these compounds are characterized by strong [M–43]⁺ peaks for C₃₈ alkenones and [M–57]⁺ for C₃₉ alkenones, which were interpreted as the loss of CH₃CO and CH₃CH₂CO groups

^{*} Corresponding author.

in methyl and ethyl ketones. C_{38} and C_{39} alkenones were thus assigned as C_{38} Me and C_{39} Et alkenones with straight alkyl chains, identical to other known alkenones(Jaraula et al., 2010). However, such fragmentation is atypical in common straight-chain alkenones (de Leeuw et al., 1980; Rontani et al., 2006b; Longo et al., 2013). The straight long-chain methyl and ethyl ketones show characteristic fragment ions at $[M-15]^+$ and $[M-29]^+$, respectively, during the ionization processes in the mass spectrometer (i.e., charge is retained preferentially on the longer alkyl chain side). One possibility that would yield strong $[M-43]^+$ and $[M-57]^+$ peaks is the presence of an alkyl substitution at the α position of a carbonyl group. This could lead to a strengthened fragmentation between carbonyl carbon and α -carbon with the formation of a stable secondary carbocation.

In this study, we performed hydrogenation on alkenone samples from Lake Van sediments to further examine structures of new C_{38} and C_{39} alkenones. Mass spectra and chromatographic behavior of these alkenones before and after hydrogenation were carefully compared to determine their structural differences with common straight-chain C_{38} Me and C_{39} Et alkenones. We also synthesized a methyl-branched C_{25} ketone to study its mass spectral fragmentation pattern and compare it with our sample compounds. Double bond positions were determined based on dimethyl disulfide derivatization reaction and subsequent mass spectral analysis.

2. Materials and methods

2.1. Sediment samples

A total of 12 sediment samples from Lake Van were obtained from IODP Bremen Core Repository. Sediment samples were from the 217 m core drilled at hole D of Ahlat Ridge site of Lake Van. This core was obtained in 2010 by the International Continental Drilling Program (ICDP) PALEOVAN project (Litt et al., 2012). Samples analyzed in this work were mainly from 10.8 to 12.6 ka based on the chronology of Stockhecke et al., 2014 (Table S1). Lake Van is endorheic and the largest lake in Turkey, with salinity ranging from 19 to 22 ppt and typical surface temperature ranging from 4 to 26 °C (Randlett et al., 2014).

2.2. Extraction of alkenones

Sediment samples from Lake Van were freeze-dried and extracted using an accelerated solvent extractor (Dionex ASE 200) with dichloromethane/methanol (9:1, v/v). Total extracts of sediment samples were then saponified using 1 mL of 1 M KOH methanol:water (v/v = 95:5) at 65 °C for 3 h. After the solution cooled to room temperature, ~1mL of 5% NaCl solution was added. The solution was then acidified to pH = 2 with HCl and extracted with 3 \times 1 mL hexane. The saponified extracts were dried and purified with silica gel (230–400 mesh, 40–63 μ m) in glass pipettes with subsequent solvent elution: hexane 4 mL, DCM 4 mL (alkenones) and methanol 4 mL.

2.3. Hydrogenation reaction

Alkenone samples were evaporated to dryness, and then dissolved in acetone. ~ 10 mg of platinum oxide was added as catalyst. Solutions were bubbled with hydrogen gas for 3 h at room temperature. Samples were then dried under nitrogen and purified with silica gel (230–400 mesh, 40–63 μm) in glass pipettes described above. Hydrogenated alkenones (i.e., alkanones) were in the DCM fraction.

2.4. Analysis of alkenones

Alkenone fractions were analyzed on a GC-FID (Gas Chromatography-Flame Ionization Detection) (Agilent 7890B) and GC-EI-MS (Gas Chromatography-Electron Ionization-Mass Spectrometry) (Agilent 7890B interfaced to a 5977 MSD) equipped with non-polar HP-1MS columns (30 m \times 250 μ m \times 0.25 μ m). The GC oven program followed that reported by Randlett et al. (2014), but with small modifications. For the analysis by GC-FID, the carrier gas was hydrogen. Samples were injected under pulsed splitless mode at 320 °C. The initial pulse pressure was 35 psi for the first 1 min. Then the purge flow to split vent was 35.0 mL min⁻¹ at 1.1 min. The flow rate (constant flow mode) was 1.5 mL min $^{-1}$. The initial oven temperature was 70 °C, then increased to 130 °C at 20 °C min⁻¹, then increased to 320 °C at 4 °C min⁻¹ and held for 20 min. For the analysis on the GC-EI-MS, samples were injected under pulsed splitless mode at 320 °C. The initial oven temperature was 40 °C for 1 min, then increased to 255 °C at 20 °C min⁻¹, then increased to 300 °C at 1 °C min $^{-1}$, then increased to 320 °C at 10 °-C min⁻¹ and held for 30 min. Samples were analyzed under fullscan mode (m/z 50 to 650). The ion source temperature was 230 °C. The electron ionization energy was 70 eV.

New C_{38} and C_{39} alkenones have previously been identified as C_{38} Me and C_{39} Et alkenones (Jaraula et al., 2010). The midpolarity poly(trifluoropropylmethylsiloxane) column has recently been found to provide much better resolutions between methyl and ethyl alkenones than non-polar GC column (Longo et al., 2013). We thus tested the chromatographic behavior of the alkenones on a GC-FID equipped with a mid-polarity RTX-200 column (105 m \times 250 μ m \times 0.25 μ m) (Zheng et al., 2017). Samples were injected under pulsed splitless mode at 320 °C. The initial pulse pressure was 35 psi for the first 1 min. Then the purge flow to split vent was 35.0 mL min⁻¹ at 1.1 min. The flow rate (constant flow mode) was 1.5 mL min⁻¹. The initial oven temperature was 50 °C for 2 min, then increased to 255 °C at 20 °C min⁻¹, then increased to 320 °C at 3 °C min⁻¹ and held for 35 min.

Due to the production of penta-unsaturated br $C_{38:5}$ Me alkenone and absence of di-unsaturated br $C_{38:2}$ Me alkenone, we devised the proxy $U_{br_{38Me}}^{K*} = \frac{br_{C_{38:3}}Me - br_{C_{38:5}}Me}{br_{C_{38:3}}Me + br_{C_{38:5}}Me}$ based on br C_{38} Me alkenones to compare their temperature sensitivity with that of $U_{37}^{K} = \frac{C_{37:2}Me - C_{37:3}Me}{C_{37:2}Me + C_{37:3}Me}$ which is based on common straight-chain C_{37} Me alkenones.

2.5. Preparation and analysis of mono-dimethyl disulfide-alkenone derivatives

Mono-dimethyl disulfide (DMDS)-alkenone derivatives were prepared following the procedure reported in Richter et al. (2017) with minor modifications. Lake Van alkenone samples were dried and dissolved in 50 μL hexane. 40 μL of iodine solution (100 mg I_2 in 1 mL Et $_2$ O) and 200 μL DMDS were then added to initiate the reaction. After flushing with N_2 for 10 s, the reaction mixture was held at 0 °C for 2 h. The reaction was stopped using 300 μL 5% sodium thiosulfate in deionized water. Products were extracted into hexane. The organic phase was transferred to a clean vial. Anhydrous sodium sulfate was added, and then allowed to sit for 30 s. The resulting reaction mixture was isolated, dried, dissolved in DCM and immediately analyzed by GC–MS.

The obtained mono-DMDS-alkenone derivatives were analyzed on a GC-EI-MS (Gas Chromatography-Electron Ionization-Mass Spectrometry) (Agilent 7890B interfaced to 5977 MSD) equipped with a non-polar HP-1MS column (30 m \times 250 $\mu m \times$ 0.25 μm). Samples were injected under pulsed splitless mode at 320 °C. The flow rate (constant flow mode) was 1.5 mL min $^{-1}$. The initial oven temperature was 40 °C for 1 min, then increased to 280 °C

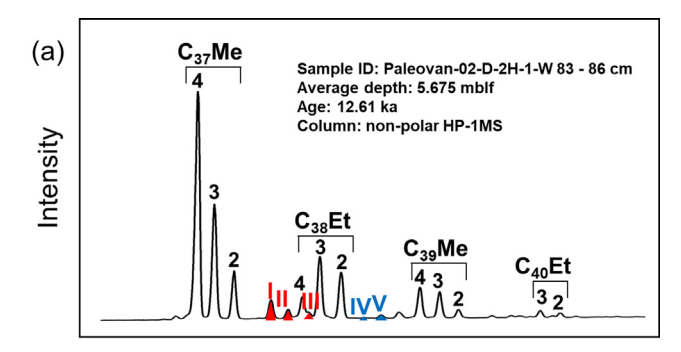
at 20 °C min⁻¹, then increased to 325 °C at 1 °C min⁻¹ and held for 30 min. Samples were analyzed under full-scan mode. The ion source temperature was 230 °C. The electron ionization energy was 70 eV. The mass range was from m/z 50 to 750.

2.6. Synthesis of brC₂₅Me branched ketone

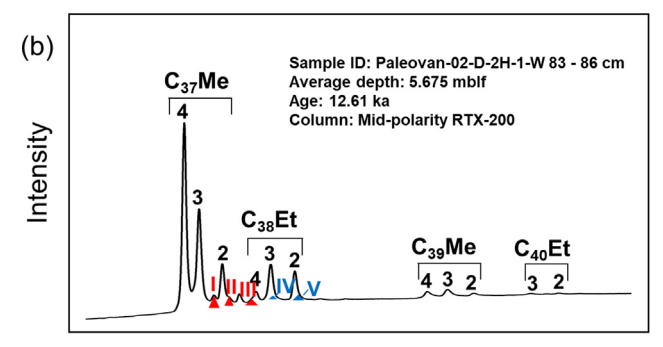
Chlorotrimethylsilane (TMSCl, 2 equiv.) was added to a stirred solution of sodium bromide (NaBr, 2 equiv.) in dry dimethylformamide (0.4 M) under nitrogen. The mixture was stirred at room temperature for 30 min to generate bromotrimethylsilane (TMSBr) in situ. 2-butanone (1 equiv.) and triethylamine (2 equiv.) were added to the mixture. The resulting mixture was stirred at room temperature for 30 h. The reaction mixture was poured into n-pentane and washed successively with saturated sodium bicarbonate solution and water. The organic layer was dried over sodium sulfate and concentrated by a rotary evaporator. The residue was distilled under normal pressure to give the corresponding silyl enol ether (b. p.110–120 °C/760 mm Hg).

$$\begin{array}{c|c} Si-CI & \begin{array}{c} NaBr \\ \hline DMF \end{array} & \begin{bmatrix} Si-Br \end{array} & \begin{array}{c} O \\ NEt_3 \end{array} & \begin{array}{c} OTMS \\ (Major) \end{array}$$

The obtained silyl enol ether (1 equiv.) was dissolved in tetrahydrofuran (THF) and hexamethylphosphoramide (HMPA) (5:1, v/v). After the solution was cooled to -78 °C, methyllithium (LiCH₃, 1 equiv.) solution was added dropwise. The resulting mixture was stirred at 0 °C for 1 h. Then the mixture was cooled to -78 °C again before straight-chain $C_{21}H_{43}I$ (2 equiv.) was added and reacted at 30 °C for 12 h to give brC₂₅Me. The reaction mixture was poured into NH₄Cl aqueous solution and extracted with ethyl acetate (EtOAc). The organic layer was dried over sodium sulfate, concentrated, and purified via column chromatography (0–1% EtOAc/Hexane). The yield for methyl-branched ketones is 73% (67% brC₂₅Me and 6% shorter chain brC₂₃Me) based on GC-FID analysis (Fig. S1a, 1H NMR in Fig. S1b). Impurities include straight-chain ethyl ketones (7% C₂₅Et and 1% C₂₃Et) and other un-identified compounds based on GC-MS analysis (Fig. S2).



Retention time



Retention time

Fig. 1. Gas chromatograms showing the alkenone distribution of sediment sample from Lake Van at 5.675 mblf (meters below lake floor). These analyses were performed on a GC-FID equipped with a non-polar poly(dimethylsiloxane) HP-1MS column (a) and a mid-polarity poly(trifluoropropylmethylsiloxane) RTX-200 column (b). New C₃₈ alkenones were labeled as compound I, II and III (red color). New C₃₉ alkenones were labeled as compound IV and V (blue color). Numbers above each peak in the chromatogram are the number of C = C bonds in corresponding compounds. (For interpretation of the references to color in this figure legend, the reader is referred to the web version of this article.)

(compounds IV-V) elute between C_{38} Et and C_{39} Me alkenones. Partial co-elution is observed between $C_{38:4}$ Et and tri-unsaturated new C_{38} alkenone (compound III) (Fig. 1a). With the mid-polarity RTX-200 column, more significant co-elutions are observed between new alkenones and C_{37} Me and C_{38} Et alkenones (Fig. 1b).

$$\underbrace{\begin{array}{c} \text{OTMS} \\ \text{(Major)} \end{array}}^{\text{OTMS}} \underbrace{\begin{array}{c} \text{LiCH}_3 \\ \text{THF/HPMA 5/1} \end{array}}_{\text{(Major)}} \underbrace{\begin{array}{c} \text{OLi} \\ \text{(Major)} \end{array}}_{\text{(Major)}} \underbrace{\begin{array}{c} \text{C}_{21}\text{H}_{43}\text{H} \\ \text{(Major)} \end{array}}_{\text{(Major)}} \underbrace{\begin{array}{c} \text{C}_{21}\text{H}_$$

3. Results and discussion

3.1. Gas chromatographic behavior of the new C_{38} and C_{39} alkenones

We analyzed Lake Van alkenones using two different GC stationary phases: (1) non-polar poly(dimethylsiloxane) HP-1MS and (2) mid-polarity poly(trifluoropropylmethylsiloxane) RTX-200 (Longo et al., 2013). The non-polar column shows better resolution of new C_{38} and C_{39} alkenones from conventional alkenones than the mid-polarity column (Fig. 1a-b). With the HP-1MS column, the new C_{38} alkenones (compounds I-III) elute between C_{37} Me and C_{38} Et alkenones, whereas the new C_{39} alkenones

Tri- to penta-unsaturated C_{38} (compounds I-III) and tetra- to penta-unsaturated C_{39} alkenones (compounds IV-V) have previously been identified as straight-chain unsaturated C_{38} Me and C_{39} Et alkenones (Jaraula et al., 2010). However, when analyzed with a mid-polarity RTX-200 column, the new C_{38} and C_{39} alkenones elute earlier than or co-elute with C_{38} Et alkenones (Fig. 1b), whereas the common C_{38} Me and C_{39} Et alkenones in fact elute after C_{38} Et alkenones (Fig. S3a). Such greatly shortened retention of the new C_{38} and C_{39} alkenones suggests their lower boiling point, weaker interaction with the stationary phase and thus significant structural differences from common straight-chain C_{38} Me and C_{39} Et alkenones.

3.2. Mass spectra of the new C_{38} and C_{39} alkenones

The unknown C₃₈ alkenones (compounds I-III) show significant differences in mass spectral fragmentation patterns (Fig. 2a-c) from the common straight-chain C₃₈Me alkenones (Fig. 2f). Molecular ions of the novel C_{38} alkenones at m/z 538, 540 and 542 correspond to penta- (Fig. 2a), tetra- (Fig. 2b) and triunsaturated (Fig. 2c) alkenones, respectively. Compared with straight-chain $C_{38}\text{Me}$ alkenones, the new C_{38} alkenones show higher relative abundances of the molecular ion peaks (e.g., $\sim 36\%$ of the base peak for the new tetra-unsaturated C_{38} alkenone. In contrast, the molecular ion for straight-chain C_{38:4}Me alkenones is only ~3%). As in the reported mass spectra of these new C₃₈ alkenones (Jaraula et al., 2010), we observe high abundances of [M-43]+ fragments in the mass spectra due to a loss of CH₃CO group. However, the interpretation that the strong [M-43]⁺ peaks derive from straight-chain methyl ketones (Jaraula et al., 2010) does not conform with mass spectral characteristics of common straight-chain methyl alkenones, which feature ions at $[M-18]^+$ and $[M-15]^+$ with slightly lower

abundances (Fig. 2f). The relative abundances of $[M-43]^+$ ions in common methyl alkenones are much lower than abundances in the new C_{38} alkenones: their abundances being $\sim 20\%$ of the base peak in the new C_{38} Me alkenones. In contrast, $[M-43]^+$ ions are absent (Fig. 2f) or below 1% in straight-chain methyl alkenones (e.g., 0.2% in $C_{37:4}$ Me and 0.4% in $C_{38:3}$ Me, Fig. S4).

Enhancement of $[M-43]^+$ fragmentation suggests three possibilities: (1) There is a double bond at beta position (i.e., Δ^3 , numbering from the carbonyl group), which creates allylic enhancement of the $[M-43]^+$ fragmentation. (2) There is an alkyl substitution at alpha position of the carbonyl group. Addition of an alkyl group could provide an additional induction effect for stabilizing the positively charged carbonyl group (when oxygen loses one electron during ionization) and the secondary carbocation after the loss of CH_3CO group. (3) There is a cyclic structure in the new alkenones that decreases their molecular weights by 2 amu relative to straight-chain alkenones. This cyclic structure could be at the alpha position of the carbonyl group so that the $[M-43]^+$ fragment ion is enhanced.

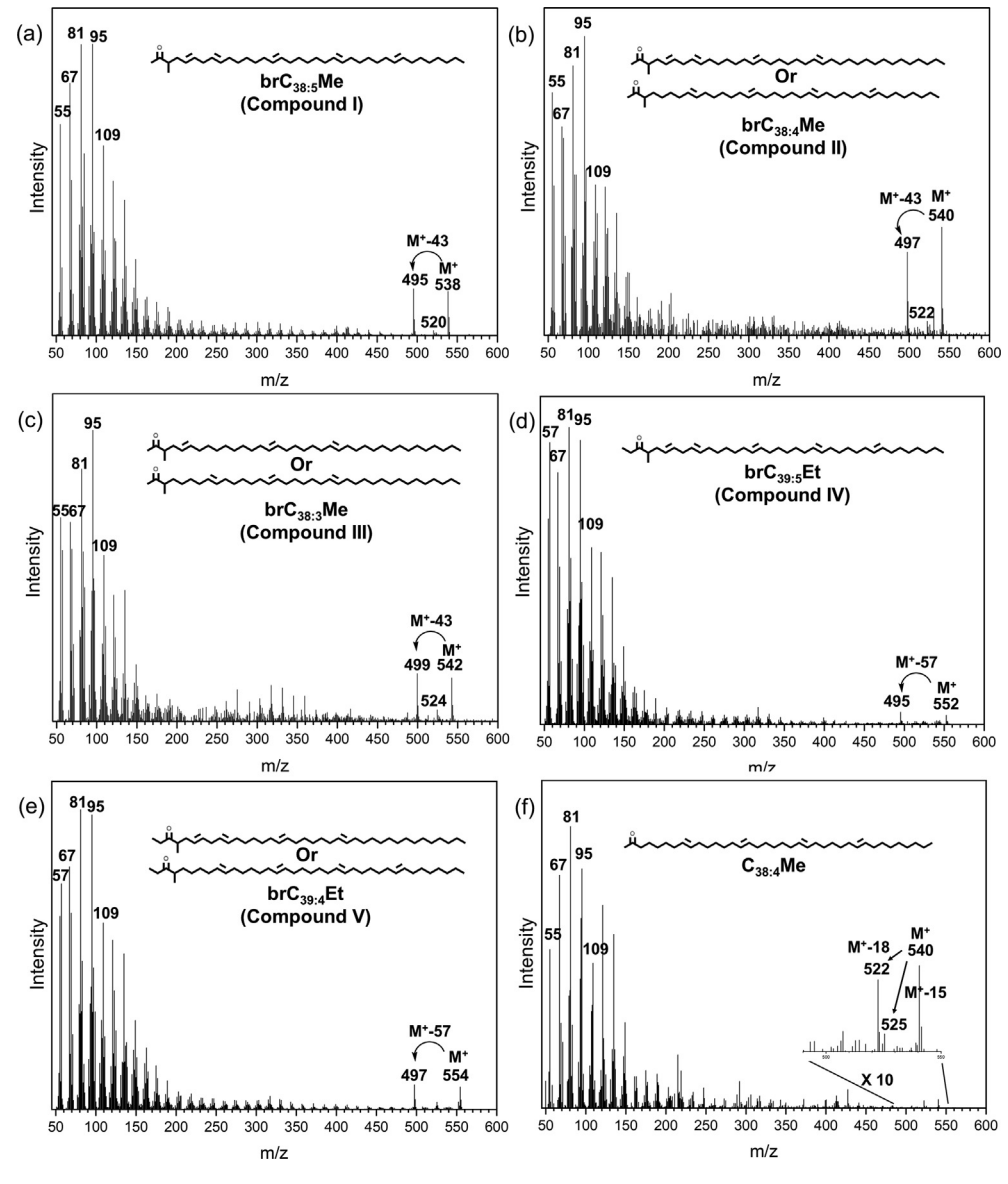


Fig. 2. Mass spectra of unsaturated alkenones including $brC_{38:5}Me$ (compound I) (a), $brC_{38:4}Me$ (compound II) (b), $brC_{38:3}Me$ (compound III) (c), $brC_{39:5}Et$ (compound IV) (d), $brC_{39:4}Et$ (compound V) (e) and $C_{38:4}Me$ (f).

Fragmentation patterns of new C_{39} alkenones are similar to the corresponding new C_{38} Me alkenones. Compound IV (Fig. 2d) and V (Fig. 2e) have molecular ions at m/z 552 and 554, suggesting they are penta- and tetra-unsaturated C_{39} alkenones, respectively. $[M-57]^+$ fragment peaks were significantly strengthened in spectra of compound IV and V, suggesting compound IV and V are new C_{39} Et alkenones with similar structures as the new C_{38} Me alkenones.

3.3. Gas chromatographic behavior and mass spectra of hydrogenated alkenones (i.e., alkanones)

Hydrogenation of samples and subsequent analysis with the RTX-200 column allowed complete resolution of new C_{38} Me alkanone (compound VI) from the C_{37} Me and C_{38} Et alkanones (Fig. 3a). The C_{38} Me and C_{39} Et alkanones have shorter retention times compared to common C_{38} Me and C_{39} Et alkanones (Fig. S3b). This clearly indicates that these new alkanones are not straight-chained.

Importantly, the mass spectra of the new C₃₈Me and C₃₉Et alkanones provide characteristic fragmentation patterns for structure

identification (Fig. 3b-c). The new C₃₈Me alkanone (compound VI) has the same molecular ion peak as C_{38} Me alkanone at m/z = 548. This excludes the possibility of the presence of a cyclic structure in new C_{38} Me alkanone. However, the peak at m/z = 72[C₄H₈O]⁺⁻ produced by McLafferty rearrangement shows an exceptional high abundance over other peaks and is the base peak in the mass spectrum of VI. On the other hand, the McLafferty rearrangement peak for straight-chain C_{38} Me $(m/z = 58 [C_3H_6O]^{+})$ has a much lower relative abundance (48% of the base peak, Fig. 3e). The McLafferty rearrangement peak in VI is 14 amu larger than the peak for straight-chain C₃₈Me alkanone, suggesting the methyl substitutions at α position in the novel alkanones (i.e., methylbranched brC38Me). The much higher abundances of McLafferty rearrangement ions in mass spectra of branched alkenones than in straight-chain alkenones result from the lower ionization energies for enol ions in the corresponding branched alkenones (Iraqi et al., 1986; Turecek et al., 1988). Unsaturated compounds I-III are therefore brC_{38:5}Me, brC_{38:4}Me and brC_{38:3}Me, respectively. The hydrogenated new C₃₉Et alkanone (compound VII) has similar fragmentation pattern with methyl-branched brC38Me (compound VI) (Fig. 3c). The McLafferty rearrangement ion at m/z 86 $[C_5H_{10}O]^+$

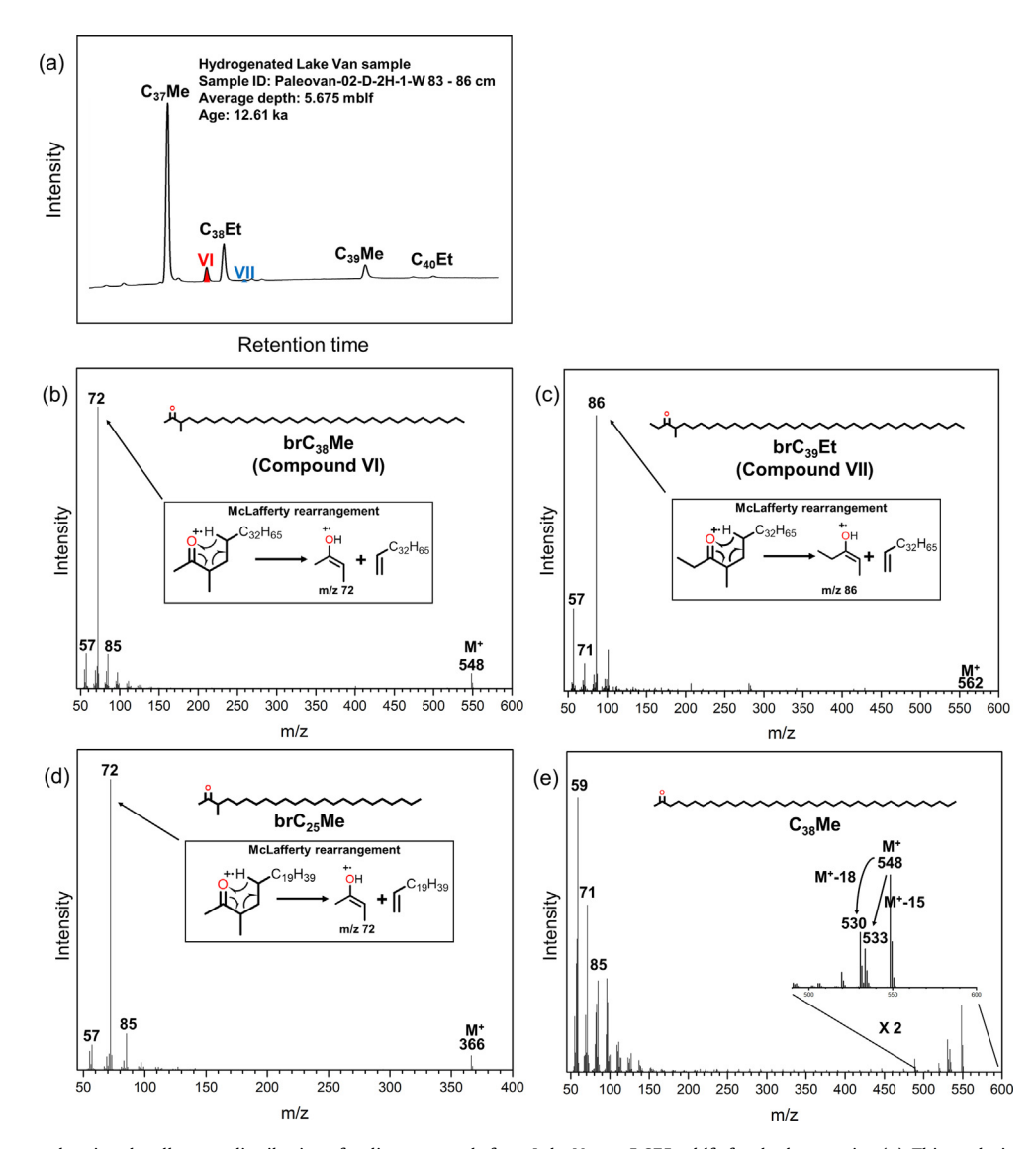


Fig. 3. Gas chromatogram showing the alkenone distribution of sediment sample from Lake Van at 5.675 mblf after hydrogenation (a). This analysis was performed on a GC-FID equipped with a mid-polarity RTX-200 column. Mass spectra of saturated ketones including hydrogenated $brC_{38}Me$ (compound VI) (b), hydrogenated $brC_{39}Et$ (compound VII) (c), synthesized $brC_{25}Me$ (d) and hydrogenated $C_{38}Me$ (e).

has much higher abundances than the other peaks, and is 14 amu larger than the rearrangement peak of methyl-branched br C_{38} Me alkanone. This indicates that the new C_{39} Et alkanone also has one methyl group at α position of carbonyl group. Compound IV and V are therefore br $C_{39:5}$ Et and br $C_{39:4}$ Et.

3.4. Mass spectrum of the synthesized analog compound

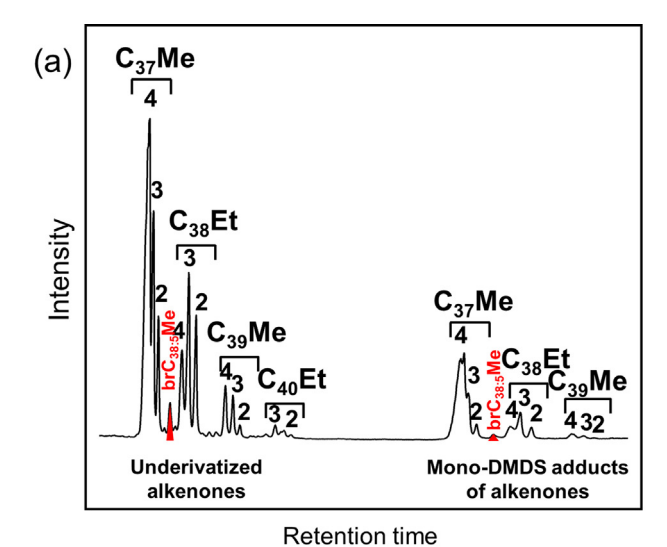
To further examine the structure assignments of the new C_{38} and C_{39} alkenones as methyl-branched alkenones, a methyl-branched C_{25} Me (br C_{25} Me) ketone with shorter chain length was synthesized. The mass spectrum of br C_{25} Me (Fig. 3d) shows similar fragmentation pattern to the hydrogenated br C_{38} Me alkanone (Fig. 3b). The peak at m/z=366 is the molecular ion peak of br C_{25} Me. The peak at m/z=366 is the molecular ion peak of br C_{25} Me. The peak at m/z=366 is the molecular ion peak of br C_{25} Me. The peak at m/z=366 is the molecular ion peak of br C_{25} Me. The peak at m/z=366 is the molecular ion peak of br C_{25} Me. The peak at m/z=366 is the molecular ion peak of br C_{25} Me and hydrogenated br C_{38} Me alkanone. The similarity of mass spectra between synthesized br C_{25} Me and hydrogenated br C_{38} Me alkanone further confirms our structure assignment.

3.5. Double bond positions in methyl-branched alkenones

Double bond positions in methyl-branched alkenones were determined based on characteristic ions in mass spectra of corresponding mono-dimethyl disulfide (DMDS) adducts (Fig. 4). Alkenones have similar elution orders before and after DMDS derivatization reaction, with DMDS adducts of $brC_{38:5}Me$ ($brC_{38:5}Me$ -DMDS) eluting between corresponding adducts of $C_{37}Me$ and $C_{38}Et$ alkenones (Fig. 4a). $brC_{38:5}Me$ -DMDS adducts have characteristic ions at m/z 632 ([M]*), m/z 585 due to a loss of SCH₃ group ([M-47]*) and ions at m/z 569 possibly due to the loss of a CH₃SO group ([M-63]*). Similar fragmentation patterns have also been observed in other alkenone-DMDS adducts (e.g., $C_{37:2}Me$ -DMDS and $C_{38:4}Et$ -DMDS, Fig S5) (Dillon et al., 2016; Zheng et al., 2016).

Cleavage of the carbon-carbon single bond caused by the reaction between C = C and DMDS vields two fragment ions for assigning original double bond positions (Dillon et al., 2016). We observe characteristic pairs of ions at m/z 159 and 473 (corresponds to Δ^{28}), 377 and 255 (Δ^{21}), 281 and 351 (Δ^{14}), 185 and 447 (Δ^7) in the DMDS adducts of brC_{38:5}Me (Fig. 4b). The ion at m/z 185 (C₁₀H₁₇OS) suggests there is one additional double bond (i.e., the fifth double bond in $brC_{38:5}Me$) before Δ^7 . The ion at m/z145 could be easily identified in the mass spectrum (26% of the base peak), which suggests the fifth double bond at Δ^4 position. On the other hand, the ion at m/z 145 has much lower abundances in DMDS adducts of C37:2Me (1% of the base peak) and C_{38:4}Et alkenones (6% of the base peak) that elute close to the $brC_{38:5}Me$ alkenone (Fig. S5). Another ion corresponding to Δ^4 double bond at m/z 487 has relatively low abundance. This may be related to the favorable charge retention on the fragment containing the carbonyl group, which has also been observed in DMDS adducts of other straight-chain alkenones (e.g., C_{37:2}Me-DMDS and C_{38:4}Et-DMDS, Fig S5) (Dillon et al., 2016; Zheng et al., 2016).

We attempted to further confirm the double bond positions in branched alkenones via derivatization with cyclobutylamine (Dillon et al., 2016). Corresponding amine adducts stabilize charges during ionization and thus yield characteristic ions of original double bond positions (Dillon et al., 2016). However, we failed to obtain cyclobutylamine adducts of branched alkenones, while other straight-chain alkenones reacted with cyclobutylamine successfully (Fig. S6). This can be readily explained by the steric hinderance caused by the methyl group at α position in branched alkenones, which prevent the nucle-



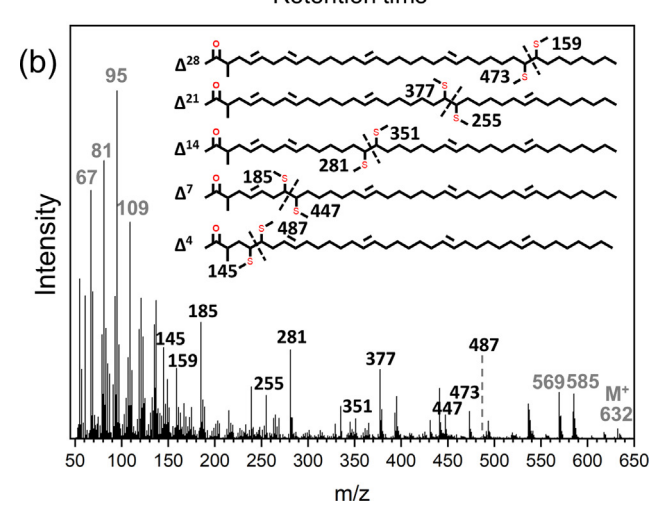


Fig. 4. Chromatogram showing the distribution of alkenone-dimethyl disulfide derivatives using a combined alkenone sample from Lake Van sediments extracted in this work (a). Mass spectrum of dimethyl disulfide derivatives of $brC_{38:5}Me$ branched alkenone (b). Numbers above each peak in the chromatogram are the number of C = C bonds in corresponding compounds.

ophilic attack of nitrogen atom in cyclobutylamine to the carbonyl carbon.

Common straight-chain alkenones contain two to four double bonds, while methyl-branched alkenones contain three to five double bonds. Notably, four double bonds in $brC_{38:5}Me$ alkenone are located at Δ^7 , Δ^{14} , Δ^{21} and Δ^{28} , respectively, identical to other tetra-unsaturated straight-chain alkenones (Dillon et al., 2016). This may suggest that methyl-branched alkenones have similar double bond positions with common straight-chain alkenones. If the unique double bond at Δ^4 position is characteristic for branched alkenone, tri- and tetra-unsaturated branched alkenones may have the same double bond positions as di- and triunsaturated straight-chain alkenones, respectively, besides the additional Δ^4 double bond in branched alkenones. Following the double bond positions in common di- and tri-unsaturated alkenones (Dillon et al., 2016), double bond positions in triunsaturated branched alkenones may thus be at Δ^4 , Δ^{14} and Δ^{21} . and at position Δ^4 , Δ^7 , Δ^{14} and Δ^{21} for tetra-unsaturated branched alkenones. However, we cannot exclude the possibility based on our data that tri- and tetra-unsaturated branched alkenones share the same double bond positions as straight-chain tri- (Δ^7, Δ^{14}) and Δ^{21}) and tetra-unsaturated alkenones (Δ^7 , Δ^{14} , Δ^{21} and Δ^{28}).

3.6. Putative biosynthetic pathways of methyl-branched alkenones

We propose a biosynthetic pathway for branched alkenones by modifying the previously proposed biosynthetic pathways for straight-chain alkenones (Rontani et al., 2006a; Zheng et al., 2016) (Fig. 5a-b). Similar to C₃₇Me and C₃₈Et alkenones, synthesis of branched alkenones could start from acetyl-SCoA, which is subsequently elongated with 16 malonyl-SCoA to obtain a carbon chain with 34 carbon atoms. For common C₃₇Me and C₃₈Et alkenones, this carbon chain is further elongated with one more malonyl-SCoA to produce a carbon chain with 36 carbon atoms. This carbon chain ends with the reaction with another methylmalonyl-SCoA/malonyl-SCoA and successive decarboxylation to produce ethyl/methyl alkenones (Fig. 5c-d) (Rontani et al., 2006a). To explain the methyl branches at the α position of carbonyl group in brC₃₈Me and brC₃₉Et alkenones, we hypothesize that the carbon chain with 34 carbon atoms is further elongated with methylmalonyl-SCoA, instead of malonyl-SCoA, to produce a methyl-branched carbon chain with 37 carbon atoms. This is similar to the synthetic pathway of branched fatty acids where the involvement of methylmalonyl-SCoA during chain elongation will result in methyl branches on the carbon chain (Dewulf et al., 2019).

For straight-chain alkenones, double bond positions on the carbon chain are determined by specific desaturases targeting Δ^7 , Δ^{14} , Δ^{21} and Δ^{28} positions (Rontani et al., 2006a; Zheng et al., 2016; Endo et al., 2018). To explain the double bond in branched alkenones at Δ^4 position, we hypothesize the involvement of an additional desaturase targeting the Δ^4 position. Such a Δ^4 desaturase

has been reported in the synthesis of docosahexaenoic acid (DHA, $C_{22:6}$ with double bonds at Δ^4 , Δ^7 , Δ^{10} , Δ^{13} , Δ^{16} , Δ^{19}) by *Isochrysis galbana* (Pereira et al., 2004; Shi et al., 2012), a well-known alkenone producer found in lacustrine and coastal areas (Theroux et al., 2010).

3.7. Downcore variations in the unsaturation degrees and percentages of brC_{28} Me alkenones in Lake Van

 U_{br38Me}^{K*} shows similar changes with U_{37}^{K} in Lake Van for the past 270 ka (Fig. 6a). Furthermore, U_{br38Me}^{K*} values correlate linearly with values of U_{37}^{K} in samples analyzed in this study between 10.8 and 12.8 ka (R^2 = 0.99, Fig. 6b). The correlation between U_{br38Me}^{K*} and U₃₇ is slight weaker when published data points are also included $(R^2 = 0.72, Fig. S7)$, probably due to the compound coelution issue and contribution of multiple alkenone producers to the overall alkenone profiles. The reasonably good correlation between U_{br38Me}^{K*} and U_{37}^{K} indicates that the unsaturation degree of $brC_{38}Me$ alkenones is also sensitive to temperature variations, similar to other straight-chain alkenones. We note that the percentage of brC38Me over total alkenones reaches high values in cool stages such as MIS 5b, 6a, 6c and periods with a drop of $U^{K\ast}_{br38Me}$ and U^{K}_{37} values (e.g., MIS 7b-d, Fig. 6a), suggesting colder conditions or related factors (e.g., reduced light intensity due to ice coverage) may promote the production of branched alkenones.

Though the actual producers of branched alkenones have not been determined, brC₃₈Me may be powerful biomarkers for tem-

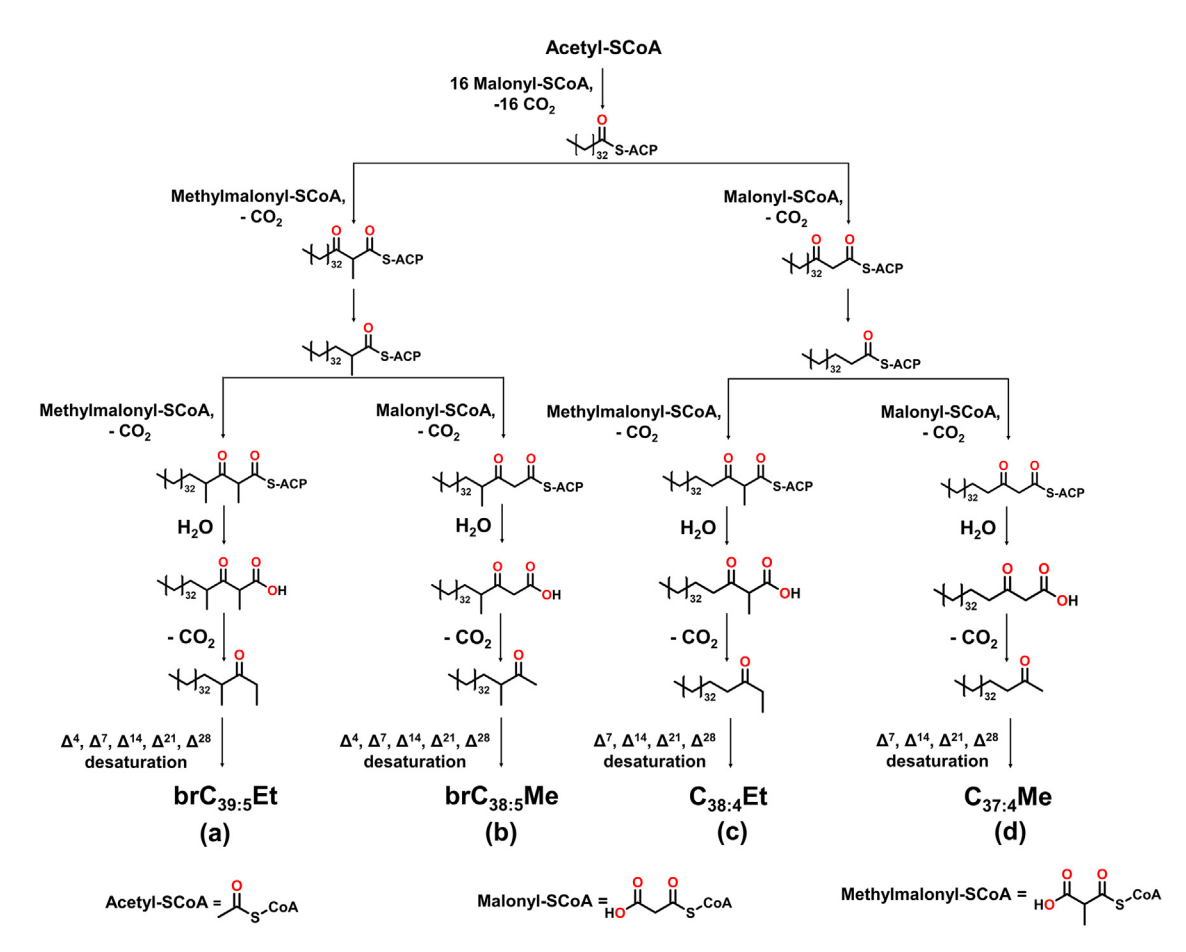


Fig. 5. Putative biosynthetic pathways of brC_{38:5}Me (b) modified based on the proposed biosynthetic pathways of C_{38:4}Et (c) and C_{37:4}Me (d) alkenones by Rontani et al., 2006a, 2006b and Zheng et al., 2016.

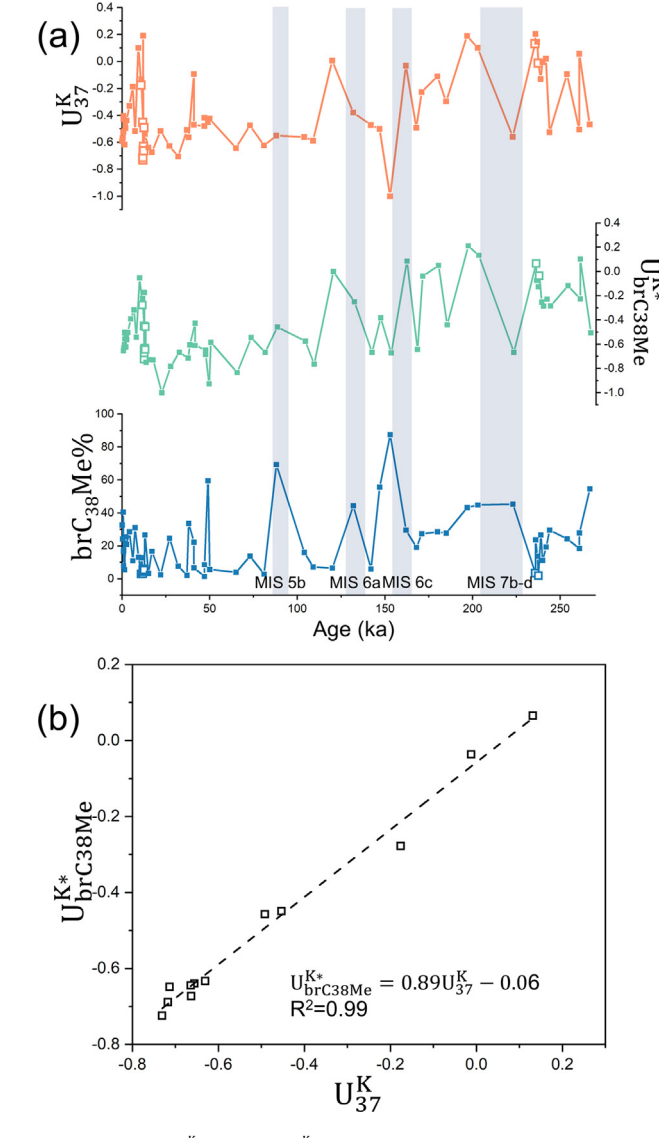


Fig. 6. Changes of U_{37}^K (orange), $U_{br38Me}^{K^*}$ (green) and percentage of $brC_{38}Me$ over total alkenones (blue) in the past 270 ka of Lake Van (a), using the published data (solid rectangle) (Randlett et al., 2014) and samples analyzed in this study (open rectangle). Correlation between U_{37}^K and $U_{br38Me}^{K^*}$ values in samples analyzed in this work (b). The nomenclature and assignment of Marine Isotope Stages (MIS) follow Pickarski and Litt, 2017 and Railsback et al., 2015. (For interpretation of the references to color in this figure legend, the reader is referred to the web version of this article.)

perature reconstructions in lacustrine and coastal areas with mixed alkenone production. Application of U_{37}^{K} and $U_{37}^{K'}$ is challenging in these areas because C₃₇Me alkenones are produced by several different alkenone-producers with different temperature calibrations (Zheng et al., 2019). If these branched alkenones are only produced by one Isochrysidales species, brC38Me alkenones would be able to provide temperature records without interference from other species. In Lake Van, there are only one or two dominant operational taxonomic units (OTUs) with much higher abundances than other OTUs in each period (Randlett et al., 2014), which may explain the high correlation between U_{br38Me}^{K*} and U_{37}^{K} . However, in sites where two or more species contribute significantly to the overall alkenone profiles, a larger deviation between U_{br38Me}^{K*} and U_{37}^{K} may be expected. Under this scenario, U_{br38Me}^{K*} could be a more reliable proxy than U_{37}^{K} (and $U_{37}^{K'}$) for temperature reconstructions.

4. Conclusions

We demonstrate that new C_{38} and C_{39} alkenones found in Lake Van and Lake Fryxell are methyl-branched alkenones (br C_{38} Me and br C_{39} Et). Previous assignments of these compounds as straight-chain C_{38} Me and C_{39} Et are incorrect. Double bond positions, determined based on mass spectrum of corresponding DMDS adducts, are Δ^4 , Δ^7 , Δ^{14} , Δ^{21} and Δ^{28} for penta-unsaturated branched alkenones. U_{br38Me}^{K*} based on br C_{38} Me alkenones has a similar trend as U_{37}^{K} over the past 270 ka in Lake Van. This suggests the high temperature sensitivity of branched alkenones, as for straight-chain alkenones. Temperature proxies based on branched alkenones may be more reliable than U_{37}^{K} and $U_{37}^{K'}$ in sites with multiple alkenone-producing haptophytes.

Declaration of Competing Interest

The authors declare that they have no known competing financial interests or personal relationships that could have appeared to influence the work reported in this paper.

Acknowledgments

This work was supported by the United States National Science Foundation awards to Y.H. (EAR-1762431). We are also grateful for the comments from two anonymous reviewers, which helped us improve the manuscript.

Appendix A. Supplementary material

Supplementary data to this article can be found online at https://doi.org/10.1016/j.orggeochem.2021.104243.

References

Brassell, S.C., Eglinton, G., Marlowe, I.T., Pflaumann, U., Sarnthein, M., 1986. Molecular stratigraphy: a new tool for climatic assessment. Nature 320, 129–133

D'Andrea, W.J., Huang, Y., Fritz, S.C., Anderson, N.J., 2011. Abrupt Holocene climate change as an important factor for human migration in West Greenland. Proc. Natl. Acad. Sci. 108, 9765–9769.

Brassell, S.C., Dumitrescu, M., The ODP Leg 198 Shipboard Scientific Party, 2004. Recognition of alkenones in a lower Aptian porcellanite from the west-central Pacific. Organic Geochemistry 35, 181–188.

de Leeuw, J., vd Meer, F., Rijpstra, W., Schenck, P., 1980. On the occurrence and structural identification of long chain unsaturated ketones and hydrocarbons in sediments. Physics and Chemistry of the Earth 12, 211–217.

Dewulf, J.P., Gerin, I., Rider, M.H., Veiga-da-Cunha, M., Van Schaftingen, E., Bommer, G.T., 2019. The synthesis of branched-chain fatty acids is limited by enzymatic decarboxylation of ethyl- and methylmalonyl-CoA. Biochem. J 476, 2427–2447.

Dillon, J.T., Longo, W.M., Zhang, Y., Torozo, R., Huang, Y., 2016. Identification of double-bond positions in isomeric alkenones from a lacustrine haptophyte. Rapid Commun. Mass Spectrom. 30, 112–118.

Endo, H., Hanawa, Y., Araie, H., Suzuki, I., Shiraiwa, Y., 2018. Overexpression of Tisochrysis lutea Akd1 identifies a key cold-induced alkenone desaturase enzyme. Sci. Rep. 8, 11230.

Farrimond, P., Eglinton, G., Brassell, S.C., 1986. Alkenones in Cretaceous black shales, Blake-Bahama Basin, western North Atlantic. Org Geochem. 10, 897–903.

Jaraula, C.M.B., Brassell, S.C., Morgan-Kiss, R.M., Doran, P.T., Kenig, F., 2010. Origin and tentative identification of tri to pentaunsaturated ketones in sediments from Lake Fryxell, East Antarctica. Org Geochem. 41, 386–397.

Iraqi, M., Pri-Bar, I., Lifshitz, C., 1986. Electron impact ionization of unstable enols: H_2C =CHOH, H_2C =C(OH)-CH $_3$ and H_2C =C(OH)-C $_2H_5$. Org. Mass Spectrom. 21, 661–664.

Liao, S., Yao, Y., Wang, L., Wang, K.J., Amaral-Zettler, L., Longo, W.M., Huang, Y., 2020. C_{41} methyl and C_{42} ethyl alkenones are biomarkers for Group II Isochrysidales. Org Geochem. 147, 104081.

Litt, T., Anselmetti, F.S., Baumgarten, H., Beer, J., Cagatay, N., Cukur, D., Damci, E., Glombitza, C., Haug, G., Heumann, G., 2012. 500,000 Years of environmental history in eastern Anatolia: the PALEOVAN drilling project. Sci. Drill. 14, 18–29.

Liu, Z., Henderson, A.C., Huang, Y., 2006. Alkenone-based reconstruction of late-Holocene surface temperature and salinity changes in Lake Qinghai, China. Geophys. Res. Lett. 33.

- Longo, W.M., Dillon, J.T., Tarozo, R., Salacup, J.M., Huang, Y., 2013. Unprecedented separation of long chain alkenones from gas chromatography with a poly(trifluoropropylmethylsiloxane) stationary phase. Org Geochem. 65, 94–102
- Longo, W.M., Huang, Y., Russell, J.M., Morrill, C., Daniels, W.C., Giblin, A.E., Crowther, J., 2020. Insolation and greenhouse gases drove Holocene winter and spring warming in Arctic Alaska. Quat. Sci. Rev. 242, 106438.
- Müller, P.J., Kirst, G., Ruhland, G., von Storch, I., Rosell-Melé, A., 1998. Calibration of the alkenone paleotemperature index U37K' based on core-tops from the eastern South Atlantic and the global ocean (60°N–60°S). Geochim. Cosmochim. Acta 62, 1757–1772.
- Pereira, S.L., Leonard, A.E., Huang, Y., Chuang, L., Mukerji, P., 2004. Identification of two novel microalgal enzymes involved in the conversion of the ω3-fatty acid, eicosapentaenoic acid, into docosahexaenoic acid. Biochem. J 384, 357– 366.
- Pickarski, N., Litt, T., 2017. A new high-resolution pollen sequence at Lake Van, Turkey: insights into penultimate interglacial-glacial climate change on vegetation history. Climate of the Past 13.
- Railsback, L.B., Gibbard, P.L., Head, M.J., Voarintsoa, N.R.G., Toucanne, S., 2015. An optimized scheme of lettered marine isotope substages for the last 1.0 million years, and the climatostratigraphic nature of isotope stages and substages. Quat. Sci. Rev. 111, 94–106.
- Randlett, M.E., Coolen, M.J.L., Stockhecke, M., Pickarski, N., Litt, T., Balkema, C., Kwiecien, O., Tomonaga, Y., Wehrli, B., Schubert, C.J., 2014. Alkenone distribution in Lake Van sediment over the last 270 ka: influence of temperature and haptophyte species composition. Quat. Sci. Rev. 104, 53–62.
- Rontani, J.-F., Prahl, F.G., Volkman, J.K., 2006a. Re-examination of the double bond positions in alkenones and derivatives: biosynthetic implications. J. Phycol. 42, 800–813.
- Rontani, J.F., Prahl, F.G., Volkman, J.K., 2006b. Characterization of unusual alkenones and alkyl alkenoates by electron ionization gas chromatography/mass spectrometry. Rapid Commun. Mass Spectrom. 20, 583–588.

- Rosell-Melé, A., Comes, P., 1999. Evidence for a warm Last Glacial Maximum in the Nordic seas or an example of shortcomings in U37K' and U37K to estimate low sea surface temperature? Paleoceanography 14, 770–776.
- Shi, T., Yu, A., Li, M., Ou, X., Xing, L., Li, M., 2012. Identification of a novel C₂₂-Δ4-producing docosahexaenoic acid (DHA) specific polyunsaturated fatty acid desaturase gene from *Isochrysis galbana* and its expression in *Saccharomyces cerevisiae*. Biotechnol. Lett. 34, 2265–2274.
- Stockhecke, M., Kwiecien, O., Vigliotti, L., Anselmetti, F.S., Beer, J., Çağatay, M.N., Channell, J.E., Kipfer, R., Lachner, J., Litt, T., 2014. Chronostratigraphy of the 600,000 year old continental record of Lake Van (Turkey). Quat. Sci. Rev. 104, 8– 17
- Turecek, F., Brabec, L., Korvola, J., 1988. Unstable enols in the gas phase. Preparation ionization, energies, and heats of formation of (E)- and (Z)-2-buten-2-ol, 2-methyl-1-propen-1-ol, and 3-methyl-2-buten-2-ol. J. Am. Chem. Soc. 110, 7984-7990.
- Theroux, S., D'Andrea, W.J., Toney, J., Amaral-Zettler, L., Huang, Y., 2010. Phylogenetic diversity and evolutionary relatedness of alkenone-producing haptophyte algae in lakes: Implications for continental paleotemperature reconstructions. Earth Planet. Sci. Lett. 300, 311–320.
- Tzanova, A., Herbert, T.D., 2015. Regional and global significance of Pliocene sea surface temperatures from the Gulf of Cadiz (Site U1387) and the Mediterranean. Global Planet. Change 133, 371–377.
- Zheng, Y., Dillon, J.T., Zhang, Y., Huang, Y., 2016. Discovery of alkenones with variable methylene-interrupted double bonds: implications for the biosynthetic pathway. J. Phycol. 52, 1037–1050.
- Zheng, Y., Tarozo, R., Huang, Y., 2017. Optimizing chromatographic resolution for simultaneous quantification of long chain alkenones, alkenoates and their double bond positional isomers. Organic Geochemistry 111, 136–143.
- Zheng, Y., Heng, P., Conte, M.H., Vachula, R.S., Huang, Y., 2019. Systematic chemotaxonomic profiling and novel paleotemperature indices based on alkenones and alkenoates: Potential for disentangling mixed species input. Org Geochem. 128, 26–41.